Int. J. Heat Mass Transfer. Vol. 34, No. 4/5, pp. 1067–1082, 1991
Printed in Great Britain

0017-9310/91 $3.00+0.00

Measurements and calculations of rough-wall heat transfer in the turbulent boundary layer

M. H. HOSNI, HUGH W. COLEMAN and ROBERT P. TAYLOR
Thermal & Fluid Dynamics Laboratory, Mechanical and Nuclear Engineering Department, Mississippi State University, Mississippi State, MS 39762, U.S.A.

(*Received* 20 *March* 1990 *and in final form* 4 *June* 1990)

Abstract—Experimental Stanton number results from aerodynamically smooth, transitionally rough, and fully rough turbulent boundary layer flows are presented for four surfaces—three rough and one smooth. The rough surfaces are composed of 1.27 mm diameter hemispheres spaced in staggered arrays 2, 4, and 10 base diameters apart, respectively, on otherwise smooth walls. Stanton number data are reported for zero pressure gradient incompressible turbulent boundary layer air flows which give Re_x up to 10 000 000. These data are compared with previously published results on another, similar rough surface, and it is shown that some conclusions about heat transfer behavior based on data from that single rough surface do not extend to these new surface geometries. A refined roughness element energy transport model for use in the previously published discrete element prediction method is also presented. Calculations are compared with data from the four rough surfaces with well-defined roughness elements for both constant pressure and accelerated flow cases, and it is shown that the predictions are in excellent agreement with the data.

INTRODUCTION

BOTH THE fluid dynamics and thermal characteristics of a flow field are affected by the shape and surface condition of a solid wall. The surface condition becomes particularly important in applications where roughness is an inherent feature. Many surfaces of engineering interest are rough in the aerodynamic sense. Turbine blades, missiles, re-entry vehicles, ship hulls, heat exchangers, and piping networks are examples of systems in which surface roughness can play an important role in heat transfer and skin friction. Both heat transfer and skin friction can be significantly larger for a turbulent flow over a rough surface compared with an equivalent turbulent flow over a smooth surface. In light of the importance of the effects of surface roughness and the broad applicability, there is significant engineering interest in the development of accurate predictive models for heat transfer and fluid mechanics in turbulent flow over rough surfaces. Development of such predictive models requires experimental data for a range of roughness conditions.

The work reported herein is concerned with heat transfer in smooth, transitionally rough, and fully rough flow regimes. Experiments are reported for the incompressible flow of air over three rough surfaces for a range of freestream velocities which gives Re_x up to 10 000 000. The three rough surfaces are composed of 1.27 mm diameter hemispherical elements spaced 2, 4, and 10 diameters apart, respectively, in staggered arrays on otherwise smooth walls. The data from the three rough surfaces are discussed and compared with previously published rough surface data. It is shown that the asymptotic behavior of the heat transfer data is not in general a valid measure for classification of rough-wall flow regimes, as was proposed previously based on data from a single rough surface.

The previously reported smooth wall data from this experimental facility serve as the baseline data and are presented with the rough-wall data to contrast the effects of roughness on heat transfer in the turbulent incompressible boundary layer. Moreover, the roughness element energy transport model in the previously published discrete element prediction approach has been refined and used for the predictions presented herein. Computations using the discrete element model are presented and compared with data obtained from four different rough surfaces. Both constant pressure gradient and accelerated flow cases are considered, and discrete element predictions are shown to be in excellent agreement with the data.

BACKGROUND

Experiment

The experimental study of surface roughness effects on fluid flow has its origin with the classic work of Nikuradse [1]. He concentrated his experimental efforts on the overall fluid dynamics behavior of rough-wall flows by measurements of pressure drop and velocity profile in pipes roughened with tightly sized sandgrains. He made an extensive number of experimental runs covering six sandgrain sizes with pipe Reynolds numbers ranging from 500 to 1 000 000. Nikuradse identified three regimes of fully developed pipe flow: aerodynamically smooth, transitionally rough, and fully rough. Aerodynamically smooth flow is flow over a surface that has the same resistance as

NOMENCLATURE

A	plate surface area
C_D	roughness element drag coefficient
C_f	skin friction coefficient, $2\tau_T/\rho U_\infty^2$
C_p	specific heat
d_0	roughness element base diameter
$d(y)$	local roughness element diameter
H	enthalpy
$H_{0,\infty}$	freestream stagnation enthalpy
k	roughness element height
K	thermal conductivity, and freestream acceleration parameter
K_t	equilibrium acceleration parameter
k_s	equivalent sandgrain roughness
l_m	mixing length
L	spacing of roughness elements
Nu_d	roughness element Nusselt number
P	pressure
Pr	Prandtl number
Pr_t	turbulent Prandtl number
q_c	conductive heat loss rate
q_r	radiative heat loss rate
q_R	rate of heat transfer from the roughness elements to the fluid
q_T	total rate of heat transfer from the surface to the fluid
r	recovery factor, or sphere radius
R_τ	roughness parameter, τ_R/τ_T
R_q	roughness parameter, q_R/q_T
Re_d	Reynolds number based on local roughness element diameter
Re_{k_s}	sandgrain roughness Reynolds number
Re_x	x-Reynolds number
St	Stanton number, $h/\rho C_p U_\infty$
T	local fluid static temperature
T_0	freestream stagnation temperature
T_r	freestream recovery temperature
T_{rail}	side rail temperature
T_R	roughness element temperature (this is taken equal to T_w)
T_w	wall (plate) temperature
u	mean longitudinal velocity
u^*	friction velocity, $\sqrt{(\tau_T/\rho)}$
u'	longitudinal velocity fluctuation
$\overline{u'v'}$	Reynolds shear stress factor
U_∞	freestream velocity
$(UA)_{eff}$	effective overall conductance for q_c calculation
$\overline{v'h'}$	turbulent heat flux factor
v	mean normal velocity
v'	normal velocity fluctuation
W	plate heater power
x	axial distance from nozzle exit
y	coordinate normal to surface
y^+	non-dimensional y, u^*y/ν
z	transverse coordinate.

Greek symbols

β_x	blockage factor
β_r	blockage factor
δ	boundary layer thickness
Δ_2	enthalpy thickness
ε	plate surface emissivity
μ	dynamic viscosity
ν	kinematic viscosity
ρ	density
σ	Stephan–Boltzmann constant
τ_R	apparent wall shear stress due to form drag on elements
τ_T	total wall shear stress.

Subscripts

t	turbulent
w	wall
∞	freestream.

flow over an ideal smooth surface at the same Reynolds number. The aerodynamically smooth regime, thus, is characterized by the skin friction coefficient depending on the Reynolds number of the gross flow only and being independent of roughness shape, size, density, etc. In contrast, for a fully rough pipe flow the skin friction coefficient depends solely on the character of the roughness and is entirely independent of the Reynolds number of the gross flow. The regime of flow between aerodynamically smooth and fully rough is known as transitionally rough. It is characterized by the dependence of the skin friction coefficient on both flow Reynolds number and roughness character.

The flow regime delimiter Nikuradse chose to measure the state of the flow with respect to the three regimes was the roughness Reynolds number, $Re_{k_s} = u^* k_s/\nu$, where u^* is the friction velocity and k_s the size of the sandgrains. His reported limits for the three regimes of fully developed rough surface flows were

aerodynamically smooth	$Re_{k_s} < 5$
transitionally rough	$5 < Re_{k_s} < 55$–70
fully rough	$Re_{k_s} > 55$–70.

Following Nikuradse's work, Schlichting [2] conducted experiments in a rectangular channel with the upper surface roughened and the remaining sides smooth. He studied the effects of roughness size, shape and density on the flow resistance using well-defined roughness elements and sandgrains. He related his skin friction results on well-described rough surfaces

to the results obtained by Nikuradse for sand-roughened pipes through definition of an equivalent sandgrain roughness. The equivalent sandgrain roughness, k_s, of a surface was defined as the sandgrain size in Nikuradse's experiment that gave the same flow resistance as the surface of interest at the same Reynolds number based on hydraulic radius. He proposed the use of the equivalent sandgrain roughness as a measure of the flow resistance character of a rough surface. It was Schlichting's stated purpose to use this parameter as a means of extrapolating a set of experimental resistance data to other Reynolds numbers based on Nikuradse's extensive data set.

The roughness Reynolds number as the delimiter of flow regimes and Schlichting's equivalent sandgrain roughness concept have been extensively used by many workers [3–5]. Many workers have in fact related their experimental data to that of Schlichting by implicitly introducing the equivalent sandgrain roughness into their data reduction. Recently it was shown that Schlichting had made erroneous assumptions during his data reduction which had significant effects on the results which he reported [6, 7]. References [6, 7] show that his skin friction results were too large by amounts ranging up to 73% and that his reported values of equivalent sandgrain roughness, k_s, were too high by amounts ranging from 26 to 555%. These findings caused some consternation, since practically all work since the 1930s on surface roughness effects relied significantly on either the skin friction or equivalent sandgrain roughness results as originally reported by Schlichting.

A recent comprehensive rough surface study was reported by Scaggs *et al.* [8, 9]. They investigated the effects of surface roughness on turbulent fully developed pipe flow friction factors using eleven different rough surfaces, nine of which had uniform roughness elements and two of which had non-uniform roughnesses. These surfaces covered a range of roughness element sizes, spacings and shapes, and friction factor data were acquired over a pipe Reynolds number range from 10 000 to 600 000.

In the past, most of the studies on the effects of surface roughness were concentrated on the fluid dynamics behavior of flows over rough surfaces. Much less work has been done in the field of heat transfer. The work of Nunner [10] is one of the first reported experimental studies on the heat transfer behavior of a rough surface. He used his experimental results for air flow through rough pipes to establish a single empirical relationship between the increase in Nusselt number due to roughness and the increase in the friction coefficient. Dipprey and Sabersky [11] studied heat and momentum transfer in smooth and rough tubes at various Prandtl numbers. They investigated the flow of four fluids of different Prandtl numbers through one smooth and three rough pipes with three-dimensional roughness elements and concluded that the heat transfer rate of fully developed rough-wall pipe flow varied with Prandtl number. The other early rough-wall heat transfer studies for internal flows are summarized by Sood and Johnson [12] and by Norris [13]. Some sources of early rough-wall heat transfer data are referenced by Yaglom and Kader [14].

A series of experimental studies at Stanford University [15–18], reported data sets for a well-defined rough surface that contain heat transfer and skin friction distributions and velocity, temperature and Reynolds stress profiles. However, these data sets are for a single rough surface which was comprised of spheres of the same size packed in the most dense array and thus do not provide information on the effects of different roughness geometries.

Computation

The two basic categories in which calculation efforts have fallen are (1) the equivalent sandgrain approach and (2) the discrete element approach. While both methods require experimental input, the equivalent sandgrain approach may require experimental data on the particular surface under consideration. On the other hand, the discrete element approach incorporates more basic physics of the process and uses a more generalized empirical input. It is therefore applicable to a broader spectrum of rough surfaces without requiring surface-specific experimental data. Since the discrete element approach is used for computations reported in this paper, an overview of this method is presented next.

The discrete element approach considers the mass, momentum and energy transport processes on the collection of individual roughness elements and the smooth surface between the elements. The basic idea is to formulate a system of partial differential equations that describes the mass, momentum and energy transport for the flow over, around and between the roughness elements. In this method the roughness effects are taken as an integral part of the flow problem and not (as with the equivalent sandgrain approach) as some ill-defined boundary condition.

Schlichting [2], in the same paper in which he introduced the equivalent sandgrain roughness, briefly discussed an alternative approach similar to the discrete element approach. He proposed that the flow resistance of a rough surface be divided into two components: (1) that due to the form drag on the element, and (2) that due to the viscous shear on the smooth surface area between the roughness elements. Following Schlichting's idea, Liepmann and Goddard [19] and Lewis [20] attempted the formulation of the discrete element method with some degree of success.

In recent years, various attempts to use the discrete element approach as a basis for calculation methods have been presented [21–28]. In these papers, researchers either introduced the equivalent sandgrain roughness in their prediction models implicitly or added terms obtained from physical reasoning. No systematic derivations of these equations from first principles were reported in these references.

References [29, 30], following the basic idea of Schlichting and building on the preceding works listed above, derived from first principles the discrete element approach for two-dimensional boundary layer flow that included the physical effects of roughness in the equations which govern the flow. This scheme includes the physical effects of roughness on the flow field by considering the blockage effects of roughness elements, the drag forces which the roughness elements exert on the field and the heat transfer between roughness elements and the flow. It does not rely on the definition of an equivalent sandgrain roughness. As derived, the discrete element approach in effect abandons the concept of sandgrain roughness and thereby abandons the roughness Reynolds number as the delimiter for aerodynamically smooth, transitionally rough and fully rough conditions.

The discrete element method used in this work is formulated for roughness elements with three-dimensional shapes (as opposed to transverse ribs) for which the element cross section can be approximated as circular at every height, y. Thus, the geometric description of the roughness element, $d(y)$, is easily included in this prediction scheme.

The steady (Reynolds-averaged), two-dimensional turbulent boundary layer equations presented here are for flow over a rough surface with roughness elements of uniform shape and spacing as derived in ref. [29]. The equations are

$$\frac{\partial}{\partial x}(\rho\beta_x u)+\frac{\partial}{\partial y}(\rho\beta_y v)=0 \tag{1}$$

$$\beta_x\rho u\frac{\partial u}{\partial x}+\beta_y\rho v\frac{\partial u}{\partial y}=-\frac{\partial}{\partial x}(\beta_x P)+\frac{\partial}{\partial y}\left[\beta_y\left(\mu\frac{\partial u}{\partial y}-\overline{\rho u'v'}\right)\right]-\frac{1}{2}\rho C_D d(y)\frac{u^2}{L^2} \tag{2}$$

and

$$\beta_x\rho u\frac{\partial H}{\partial x}+\beta_y\rho v\frac{\partial H}{\partial y}=\frac{\partial}{\partial y}\left[\beta_y\left(\frac{K}{C_p}\frac{\partial H}{\partial y}-\overline{\rho v'h'}\right)\right]+u\frac{\partial}{\partial x}(\beta_x P)+\beta_y\frac{\partial u}{\partial y}\left(\mu\frac{\partial u}{\partial y}-\overline{\rho u'v'}\right)+\frac{1}{2}\rho C_D\frac{d(y)}{L^2}u^3+\pi\frac{KNu_d}{L^2}(T_R-T). \tag{3}$$

Examination of equations (2) and (3) shows that empirical models for $-\overline{\rho u'v'}$, $-\overline{\rho v'h'}$, the roughness element drag coefficient $C_D(y)$, and the roughness element Nusselt number $Nu_d(y)$ are necessary for closure.

The blockage parameters β_x and β_y and the element shape descriptor $d(y)$ require no empirical fluid mechanics input as they are determined solely from the geometry of the rough surface. It was shown in ref. [29] for uniform three-dimensional roughness elements with circular cross-section that

$$\beta_x=\beta_y=1-\frac{\pi d^2(y)}{4L^2}. \tag{4}$$

Note that for $y>k$, $d(y)=0$ and both β_x and β_y become identically 1.0.

The boundary conditions for the discrete element approach for rough wall flows are identical to those for smooth wall flows. The wall location ($y=0$) is the smooth surface on which the roughness elements occur. At $y=0$, $u=v=0$ and $H=H_w$. As $y\to\infty$, $u\to U_\infty$ and $H\to H_\infty$.

The numerical solution of the discrete element equations is obtained by finite difference solution of the transformed equations in the computational plane. The transformation, finite difference scheme, and program structure are described in ref. [29]. The streamwise derivative is approximated with a first-order backwards difference. The surface normal derivatives are replaced with second-order approximations which allow the spacing between grid points to vary with distance from the wall. This allows a concentration of nodes near the wall and below the crests of the elements. In this stretched grid the ratio of any two adjacent mesh lengths is a constant.

The solution is by an iterative marching, implicit method. The solution is known at station i and is sought at station $i+1$. The implicit difference equations result in a tridiagonal coefficient matrix the inverse of which is known and can be expressed algebraically (often referred to as the Thomas algorithm). Since the equations are nonlinear, the system must be solved by iteration. A relaxation scheme is employed with a required residual less than 0.01%.

The solutions were obtained on finer and finer grids until differences were less than 1% in computed values of C_f and St. In the transformed coordinates there were typically 250 grid points across the boundary layer which corresponds to approximately 40–60 grid points below the crest of the elements. The streamwise grid spacing was typically 1 cm.

In addition, the codes were verified by comparisons with known solutions of smooth-wall laminar and turbulent flows.

The 'wall shear stress' is defined as the sum of the shear and drag forces on the wall in the mean flow direction divided by the plan area of the wall. The corresponding skin friction coefficient is then

$$C_f=\frac{(\beta_y)_w\mu\left.\frac{\partial u}{\partial y}\right|_w+\frac{1}{2}\frac{1}{L^2}\int_0^k(\rho dC_D u^2)\,dy}{\frac{1}{2}\rho_\infty U_\infty^2} \tag{5}$$

and the Stanton number is

$$St=\frac{-(\beta_y)_w\frac{K}{C_p}\left.\frac{\partial H}{\partial y}\right|_w+\frac{\pi}{L^2}\int_0^k[KNu_d(T_R-T)]\,dy}{\rho_\infty U_\infty(H_w-H_{0,\infty})}. \tag{6}$$

In order to solve equations (1)–(3), turbulence models for $-\overline{\rho u'v'}$ and $-\overline{\rho v'h'}$ and roughness models for C_D and Nu_d are required. Because of its proven predictive capability for attached boundary layer flows over smooth surfaces, the Prandtl mixing length model with van Driest damping and a constant turbulent Prandtl number is used for turbulence closure. Thus

$$-\overline{\rho u'v'} = \rho l_m^2 \left(\frac{\partial u}{\partial y}\right)\left|\frac{\partial u}{\partial y}\right| \tag{7}$$

where

$$l_m = 0.40y[1-\exp(-y^+/26)]; \quad l_m < 0.09\delta \tag{8}$$

$$l_m = 0.09\delta; \quad \text{otherwise} \tag{9}$$

and

$$-\overline{\rho v'h'} = \frac{\mu_t}{Pr_t}\frac{\partial H}{\partial y} \tag{10}$$

where

$$Pr_t = 0.9. \tag{11}$$

The roughness element C_D and Nu_d models are formulated as functions of the local element Reynolds number $Re_d = u(y)d(y)/\nu$ which includes roughness element size and shape information through $d(y)$. As discussed in ref. [29], the C_D model which gave the best overall agreement with experimental data was

$$\log C_D = -0.125\log(Re_d) + 0.375. \tag{12}$$

This model has been tested for values of Re_d up to 25 000 [8, 29] using many data sets. In particular, Scaggs *et al.* used eleven different rough surfaces, nine of which had uniform roughness elements and two of which were roughened nonuniformly. It was demonstrated that the roughness element drag coefficient model in the discrete element prediction approach gave excellent agreement with all of these data sets. Consequently, this model was used unchanged for the predictions presented in this work.

The roughness element energy transport model requires empirical input in the form of a Nusselt number, Nu_d. A $Nu_d = f(Re_d, Pr)$ model was developed [29] which was tested for roughness element Reynolds numbers up to $Re_d = 1000$, using heat transfer data from the single Stanford rough surface. In this current effort, a modified Nu_d model based on several experimental runs from four different rough surfaces was formulated using that of ref. [29] as a starting point. The modified model, which has been tested up to Re_d of about 2200, is

$$Nu_d = 1.7Re_d^{0.49}\,Pr^{0.4}. \tag{13}$$

The numerical procedure used to solve the governing equations in the discrete element approach is discussed in detail in ref. [29]. An iterative marching, implicit finite difference method, adapted from the smooth wall approach of Adams [31], was used to solve equations (1)–(3). The solution was obtained on finer and finer grids until no differences were noted in the computed values of C_f and St to three significant digits. In addition, the code was verified by comparisons with known solutions of smooth wall turbulent and laminar flows.

At this point some remarks are in order. Recall that previously the three regimes of flow over a rough surface were discussed. No mention of these regimes was made in the discussions concerning the development of either roughness element drag coefficient, C_D, or heat transfer, Nu_d, models used in the discrete element approach. All calculation methods that use the sandgrain roughness approach must take care to distinguish between these regimes, because different models are required for aerodynamically smooth, transitionally rough and fully rough flows. This brings forth the added burden of predetermination of the state of the flow. The discrete element approach does not need to make these distinctions a priori, since such information is implicitly included in the roughness element C_D and Nu_d models. Therefore, the discrete element method applies to smooth, transitionally rough and fully rough flows without prior determination of the flow regime.

Since the equivalent sandgrain concept is abandoned in the discrete element approach, the use of roughness Reynolds number for classifications of the flow regimes is no longer useful. It was suggested in ref. [29] that the ratio of the apparent shear stress due to the roughness elements to the total apparent shear stress ($R_\tau = \tau_R/\tau_T$) as calculated using the discrete element method be used to distinguish between aerodynamically smooth, transitionally rough and fully rough regimes.

As discussed previously, Scaggs *et al.* [8] investigated the effects of surface roughness on turbulent pipe flow friction factors using eleven different rough surfaces. Based on their data and the suggestions of Taylor *et al.*, they proposed that

aerodynamically smooth	$R_\tau < 0.05$–0.1
transitionally rough	0.05–$0.1 < R_\tau < 0.6$
fully rough	$R_\tau > 0.6$.

EXPERIMENTAL APPARATUS AND MEASUREMENT PROCEDURES

The experiments were performed in the Turbulent Heat Transfer Test Facility (THTTF) which is shown in Fig. 1. Complete descriptions of the facility and its qualification are presented in ref. [32]. This facility is a closed loop wind tunnel with a freestream velocity range of 6–67 m s^{-1}. The temperature of the circulating air is controlled with an air to water heat exchanger and a cooling water loop. Following the heat exchanger the air flow is conditioned by a system of honeycomb and screens.

The bottom wall of the nominally 2.4 m long by 0.5 m wide by 0.1 m high test section consists of

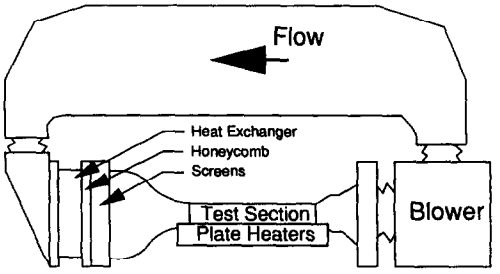

Fig. 1. Schematic of the Turbulent Heat Transfer Test Facility (THTTF).

24 electrically heated flat plates which are abutted together to form a continuous flat surface. Each nickel plated aluminum plate (about 10 mm thick by 0.1 m in the flow direction) is uniformly heated from below by a custom-manufactured rubber-encased electric heater pad. Design computations showed that, with this configuration, a plate can be considered to be at a uniform temperature. The three sets of precision machined rough test plates considered here have 1.27 mm diameter hemispherical elements spaced 2, 4, and 10 diameters apart, respectively, in staggered arrays as shown in Fig. 2. The measured average surface roughness on the 'smooth' wall portion of the plates is less than 1.6 μm, and the allowable step (or mismatch) between any two plates is 0.013 mm. The heating system is under active computer control and any desired set of plate temperatures can be maintained within the limits of the power supply. To minimize the conduction losses, the side rails which support the plates are heated to approximately the same temperature as the plates.

The top wall can be adjusted to maintain a constant freestream velocity. An inclined water manometer with resolution of 0.06 mm is used to measure the pressure gradient during top wall adjustment. Static pressure taps are located in the side wall adjacent to each plate. The pressure tap located at the second plate is used as a reference, and the pressure difference between it and each other tap is minimized. For example, the maximum pressure difference for the 43 m s^{-1} case was 0.30 mm of water.

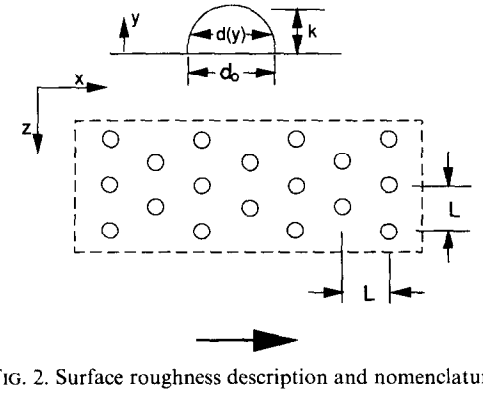

Fig. 2. Surface roughness description and nomenclature.

The boundary layer is tripped at the exit of the 19 : 1 area ratio nozzle with a 1 mm × 12 mm wooden strip. This trip location is immediately in front of the heated surface.

Before proceeding with rough surface testing with the THTTF, a series of qualification tests [32] were performed with a set of smooth test plates to insure the fitness of the test rig and the correctness of the instrumentation, data acquisition system, and data reduction procedures. Measurements in the nozzle exit plane showed the mean velocity to be uniform within about 0.5% and the freestream turbulence intensity to be less than 0.3%. Measurements 1.1 m downstream of the nozzle exit showed the spanwise variation of momentum thickness to be less than $\pm 0.5\%$. Profiles of mean temperature and velocity were in good agreement with the usual 'laws-of-the-wall'. Stanton number data for the constant wall temperature cases were in excellent agreement with the data of Reynolds *et al.* [33], which is the definitive data set on which the usual Stanton number correlations are based. The THTTF smooth wall data fall within the data scatter of this definitive data set.

Stanton number determination

The data reduction expression for the experimentally determined Stanton number is

$$St = \frac{W - (UA)_{\text{eff}}(T_w - T_{\text{rail}}) - \sigma\varepsilon A(T_w^4 - T_r^4)}{\rho C_p U_\infty A(T_w - T_0)}. \quad (14)$$

The power, W, supplied to each plate heater is measured with a precision wattmeter. The radiation heat loss, q_r, is estimated using a gray body enclosure model where the emissivity of the nickel plated aluminum is estimated as $\varepsilon = 0.11$. The conductive heat loss, q_c, is calculated using an experimentally determined effective plate conductance, $(UA)_{\text{eff}}$, which includes both side rail and back losses. The conduction losses are minimized by actively heating the side rails. Both q_r/W and q_c/W are generally in the 0.5–1% range. The density and specific heat are determined from property data for moist air using the measured values of barometric pressure and wet and dry bulb temperatures in the tunnel. The freestream velocity is measured using a Pitot probe and specially calibrated precision pressure transducers. The freestream and plate temperatures are measured using specially calibrated thermistors. The freestream total temperature, T_0, is computed using the measured freestream recovery temperature, T_r, and a recovery factor for the freestream thermistor probe of $r = 0.86$ [34]. All fluid properties are evaluated at the freestream static temperature.

The uncertainty in the experimentally determined Stanton number was estimated based on the ANSI/ASME Standard on Measurement Uncertainty [35] following the procedures of ref. [36]. For the Stanton number data in this paper, the overall uncertainty, as discussed in detail in refs. [32, 37], ranged from about 2 to 5%, depending on flow conditions.

DISCUSSION

The experimental heat transfer results obtained in the THTTF for turbulent boundary layer flow over three different well-defined rough surfaces are presented for nominal freestream velocities of 6, 12, 28, 43, 58, and 67 m s^{-1}. The previously reported smooth wall Stanton number data sets from this experimental facility serve as the baseline data for comparison with the results of rough walls. All of the THTTF data are for zero pressure gradient, constant wall temperature, incompressible, turbulent boundary layer flow of air.

The THTTF Stanton number data are also compared with the Stanford data taken on a single rough surface comprised of 1.27 mm diameter spheres packed in the most dense array. The Stanford surface and the THTTF surfaces can be considered to be in the same family of rough surfaces if one assumes that surfaces of 1.27 mm diameter hemispheres and 1.27 mm diameter spheres spaced in the most dense array appear similar to a turbulent boundary layer.

Calculations using the discrete element prediction method are compared with the data taken on the three rough surfaces in the THTTF and the data from the Stanford surface. Comparisons with the Stanford data sets include both constant pressure gradient and accelerated flow cases.

Experimental results

Stanton number data sets are presented graphically in two formats: (1) with an ordinate of St and abscissa of Re_x, and (2) with an ordinate of St and abscissa of Δ_2/k, where Δ_2 is the enthalpy thickness and k the roughness height (which corresponds to the sphere radius, r, used in the original Stanford surface data presentations). Values of Re_x were computed with the length scale (x) taken as the distance from the leading edge of the first plate. To compute Δ_2/k, the enthalpy thickness corresponding to each Stanton number was determined by numerical integration of the applicable form of the integral energy equation for the isothermal surface $St = \mathrm{d}\Delta_2/\mathrm{d}x$ [38].

In order to contrast the data for rough surfaces with the smooth wall results, each plot of rough-wall Stanton number data vs Re_x includes a curve representing the smooth wall correlation. In plots of St vs Re_x, the smooth wall Stanton number correlation expression [39]

$$St = 0.185(\log_{10} Re_x)^{-2.584} Pr^{-0.4} \qquad (15)$$

is used. The uncertainty intervals on selected data points indicate the estimated overall uncertainty limits on Stanton numbers.

Figure 3 shows a composite plot of the THTTF Stanton number data for nominal freestream velocities of 12, 28, 43, 58, and 67 m s^{-1} for the three rough surfaces and the smooth THTTF surface. This figure clearly shows the increase in Stanton number with increased roughness density. For the surface with $L/d_0 = 4$, the increase in St over the equivalent smooth wall case is about 40%; and for $L/d_0 = 2$, the increase is about 75%.

In these coordinates the smooth wall data sets corresponding to the five different freestream velocities collapse to a single curve, as expected. For the three rough surfaces, the Stanton number data sets appear to collapse to single, asymptotic curves for $U_\infty = 28$ m s^{-1} and greater. However, the Stanton numbers at $U_\infty = 12$ m s^{-1} for all three rough surfaces exhibit a distinct shift from corresponding data sets taken at higher freestream velocities.

Figure 4 shows Stanton number data sets reported by Healzer [15] and Pimenta [16] for constant wall temperature, zero pressure gradient turbulent boundary layer flows over the Stanford surface plotted in St vs Re_x coordinates. (The lines are predictions, which will be discussed later.) These data exhibit similar behavior to the data from the three THTTF rough surfaces in that the data for the highest freestream velocities appear to collapse together in these coordinates, although for this surface the data for $U_\infty = 27$ m s^{-1} fall below the higher U_∞ data rather than collapsing together with them.

The asymptotic curve for the Stanford surface falls between those of the $L/d_0 = 2$ and 4 THTTF surfaces. This seems to indicate that the magnitude of the roughness effect on heat transfer increases with decreased roughness element spacing only up to some 'roughest' spacing. As roughness element spacing is decreased more (and approaches the most densely packed configuration), the magnitude of the roughness effect on heat transfer diminishes. This is in agreement with the trends shown by Schlichting's [2] data for roughness effects on skin friction as a function of roughness element spacing.

Because these data were from only one surface, neither Healzer nor Pimenta recognized the apparent approach of the St data to a single curve in Re_x coordinates as U_∞ increased. Rather, they postulated such behavior in St vs Δ_2/r coordinates. Figure 5 shows these same Stanton number data from the Stanford surface plotted vs Δ_2/r, where r is the radius of the spherical roughness elements. (The lines are predictions, which will be discussed later.) Healzer [15] proposed that the St vs Δ_2/r coordinates are more appropriate for presenting rough-wall Stanton number results. He postulated that since his data showed no apparent velocity dependence in these coordinates, the Stanton number was a function only of Δ_2/r for all velocities.

Pimenta [16] studied both the Stanton number behavior and the turbulence characteristics of the boundary layer using the same rough porous surface. He concluded that, for the Stanford surface, Stanton number behavior was independent of Reynolds number in the fully rough flow regime. He postulated that in the fully rough regime the Stanton number data plotted in St vs Δ_2/r collapse together and this characteristic may be used to distinguish rough-wall flow regimes. He used this criterion for classification of

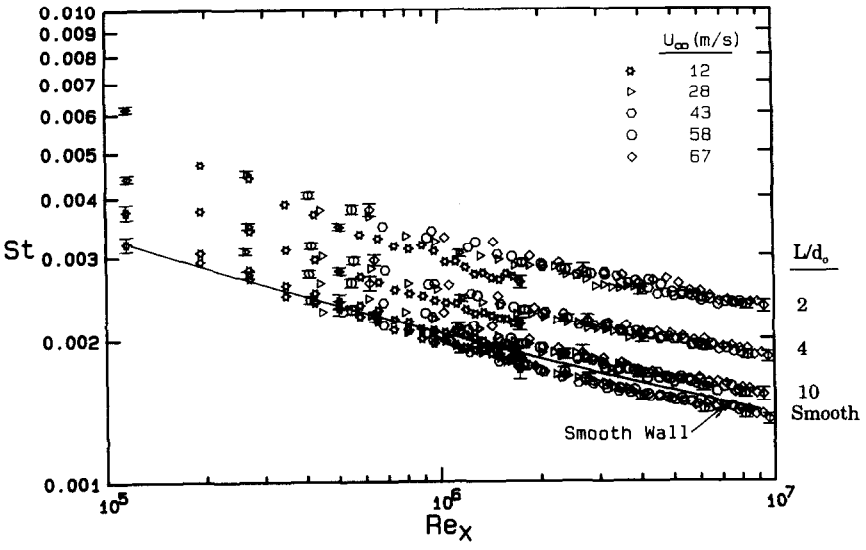

FIG. 3. Composite plot of Stanton number data vs Re_x for the THTTF smooth and rough surfaces.

his own three Stanton number runs for freestream velocities of 16, 27, and 40 m s^{-1} shown in Fig. 5. He identified the 16 m s^{-1} run as transitionally rough and the 27 and 40 m s^{-1} runs as fully rough. However, he pointed out that the difference in the data for his 16 m s^{-1} transitionally rough run and the 27 and 40 m s^{-1} fully rough runs was small when plotted in these coordinates. He supported his classification of the 16 m s^{-1} run as transitionally rough using the behavior of the $\overline{u'^2}$ profiles.

In his investigation of the Reynolds stress tensor components in fully rough and transitionally rough boundary layers, Pimenta observed that in the transitionally rough regime $\overline{u'^2}$ profiles showed qualitative characteristics similar to the smooth wall state, with a near-wall peak present. In the fully rough regime, the peak in $\overline{u'^2}$ was lowered, moved away from the wall, and spread over a larger portion of the boundary layer. He concluded that the distinctive difference in the near-wall profiles of $\overline{u'^2}$ could be used to distinguish between the transitionally rough and fully rough regimes. Ligrani [18] also reported this distinct difference in the near-wall peak in $\overline{u'^2}$ profiles, and this same near-wall behavior of $\overline{u'^2}$ profiles was observed for the three THTTF rough surfaces [37].

Pimenta's final classification of flow regimes for the Stanford surface based on both St vs Δ_2/r behavior and boundary layer structural studies was that the 9

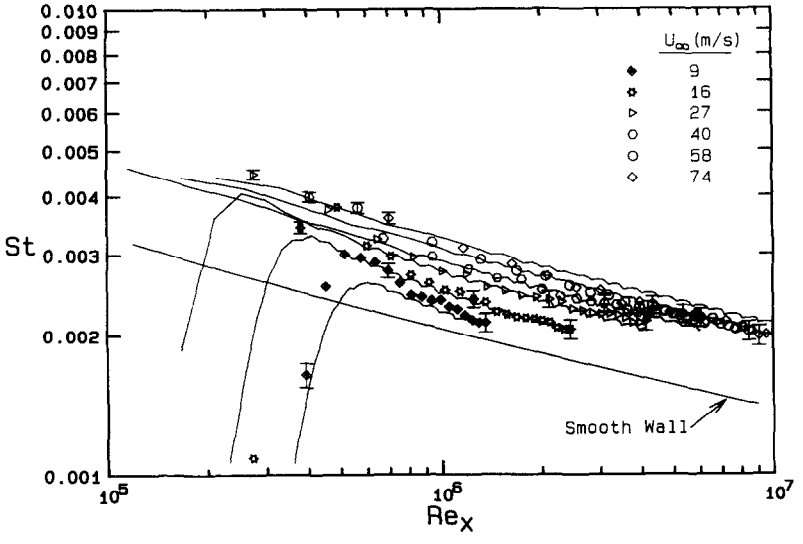

FIG. 4. Stanton number data reported by Healzer [15] and Pimenta [16] and predictions vs Re_x for Stanford surface.

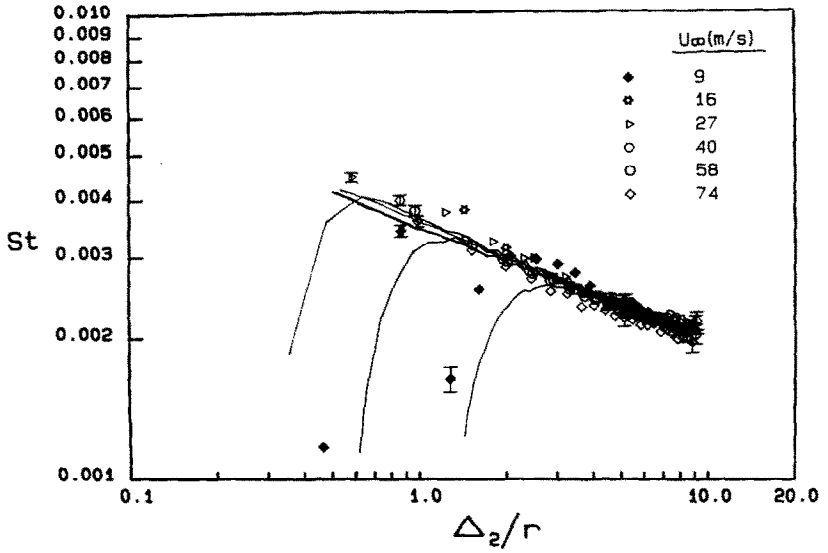

FIG. 5. Stanton number data reported by Healzer [15] and Pimenta [16] and predictions vs Δ_2/r for the Stanford surface.

and 16 m s^{-1} data were in the transitionally rough regime, and the data for $U_\infty \geqq 27$ m s^{-1} were in the fully rough regime.

Figures 6–8 present Stanton number data for the three THTTF rough surfaces, respectively, in St vs Δ_2/k coordinates. (Note that k corresponds to r for hemispherical elements, and that this value is numerically the same for the Stanford surface and the THTTF surfaces. Also, as before, the lines are predictions and will be discussed later.) Figure 6 shows the $L/d_0 = 2$ rough surface data, and only the 58 and 67 runs collapse together. If the St vs Δ_2/k criterion proposed by Pimenta were to be used, these two runs would be classified as fully rough and the others as transitionally rough. This classification could not be supported by either the criterion based on the shape of the $\overline{u'^2}$ profile or the criterion set by the magnitude of R_τ [37], both of which indicate that for $U_\infty \geqq 12$ m s^{-1}, all of the data are in the fully rough regime. The classification of flow regimes for the $L/d_0 = 10$ surface based on the behavior of St vs Δ_2/k (Fig. 8) would be even more perplexing. Again, the 58 and 67 m s^{-1} results collapse together and would be classified as in the fully rough flow regime. However, based on $\overline{u'^2}$ behavior and R_τ values none of the runs on this surface correspond to the fully rough regime.

Based on observation of the data from the three THTTF rough surfaces and the Stanford surface, it

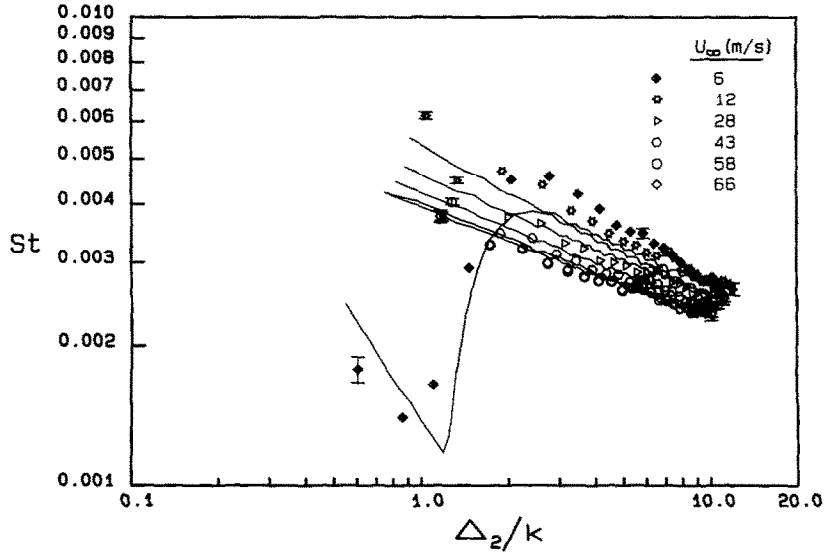

FIG. 6. The THTTF Stanton number data and predictions vs Δ_2/k for the $L/d_0 = 2$ rough surface.

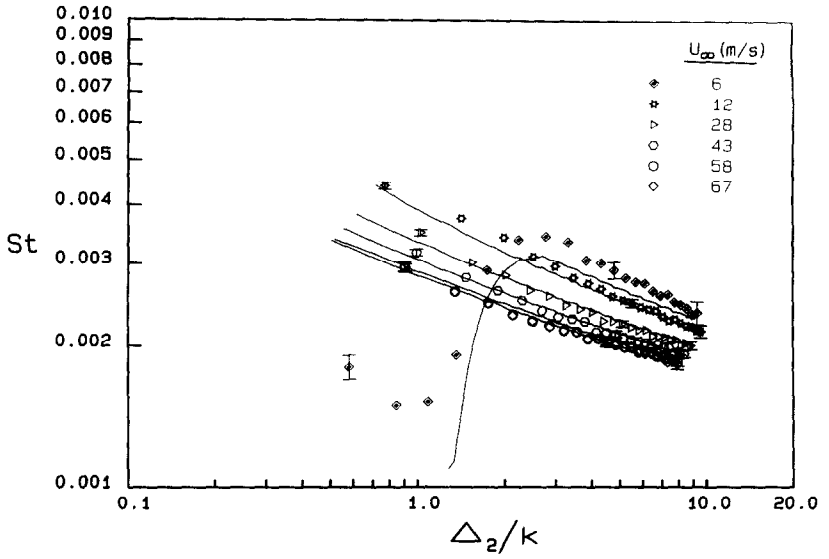

FIG. 7. The THTTF Stanton number data and predictions vs Δ_2/k for the $L/d_0 = 4$ rough surface.

appears that the previously proposed classification of roughness flow regimes based on heat transfer behavior in St vs Δ_2/k or Δ_2/r coordinates is not viable. The data do not support the idea that fully rough Stanton numbers are functions only of Δ_2/r.

Predictions

The Stanton number data for the three THTTF rough surfaces are compared with the calculations made using the discrete element prediction method in St vs Re_x coordinates in Figs. 9–11. The uncertainty bands on selected data points indicate the estimated uncertainties on the Stanton data, and the lines represent the predictions. As shown, the discrete element method predictions agree with the data extremely well over the range of roughness spacing and for aerodynamically smooth, transitionally rough and fully rough flow regimes. Corresponding comparisons in St vs Δ_2/k coordinates are shown in Figs. 6–8.

The discrete element method has also been used to make predictions corresponding to three of the investigations performed using the Stanford surface. Two of these [15, 16] reported skin friction coefficients and Stanton numbers for both transitionally rough and fully rough zero pressure gradient flow over a constant temperature rough surface. The third [17] included favorable freestream pressure gradients for both equilibrium and non-equilibrium cases. Since this surface (composed of eleven layers of 1.27 mm diameter spheres packed in the most dense array) did not have

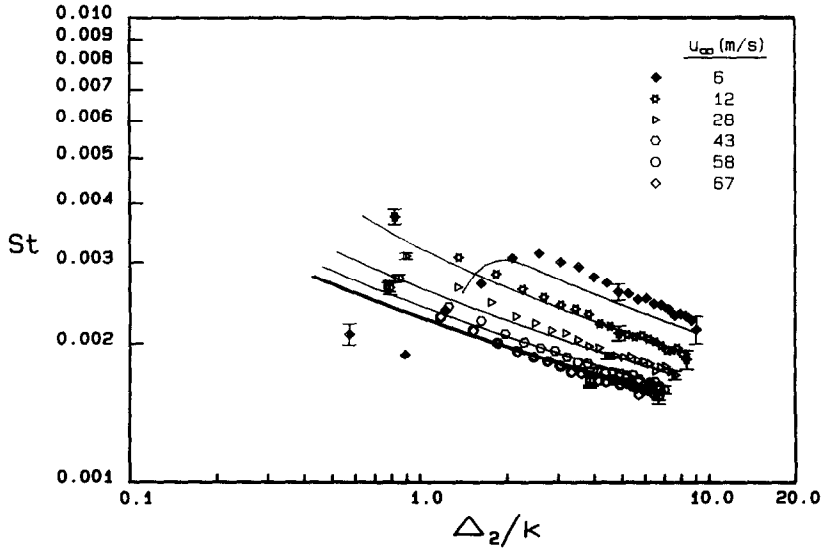

FIG. 8. The THTTF Stanton number data and predictions vs Δ_2/k for the $L/d_0 = 10$ rough surface.

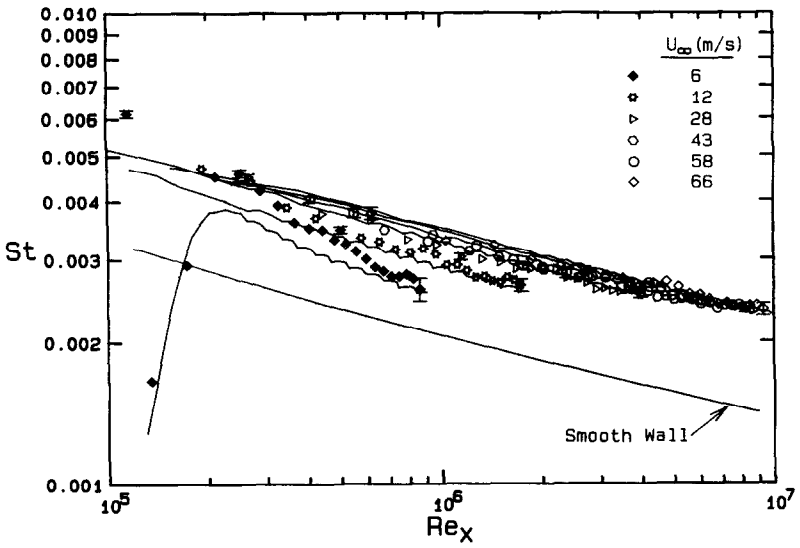

FIG. 9. The THTTF Stanton number data and predictions vs Re_x for the $L/d_0 = 2$ rough surface.

a solid base smooth wall, an effective base wall location 0.2 sphere diameter below the crests of the spherical elements as determined in ref. [29] was used in the calculations. This effective wall location allowed use of the same C_D expression for the most densely packed spheres as was used in the original development based on the surfaces tested by Schlichting [2]. It should also be noted that the correct specification for element spacing is 0.866 and 1.0 sphere diameters in the x- and z-directions, respectively.

The zero pressure gradient Stanton number data sets for the Stanford rough surface reported by Healzer [15] and Pimenta [16] are compared with calculations made with the discrete element method in Fig. 4. The calculations for freestream velocities of 9, 16, 27, 40, and 58 are in excellent agreement with the data, and for 74 m s^{-1} the discrete element model predicts Healzer's data almost within the data uncertainty of ± 0.0001 St units. Corresponding comparisons in St vs Δ_2/r coordinates are shown in Fig. 5.

Figure 12 presents comparisons between the favorable pressure gradient (accelerated flow) Stanton number data sets for the Stanford rough surface reported in ref. [17] and predictions from the discrete element method. Both equilibrium and non-equilibrium fully rough turbulent boundary layer data sets are shown. The conditions for which equilibrium exists in fully rough turbulent boundary layer flow are given in ref. [17]. The strength of the pressure gradi-

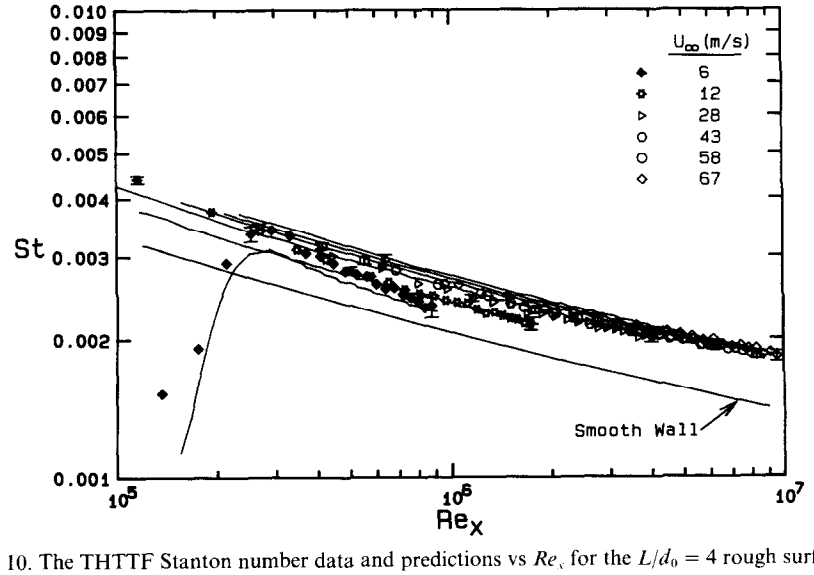

FIG. 10. The THTTF Stanton number data and predictions vs Re_x for the $L/d_0 = 4$ rough surface.

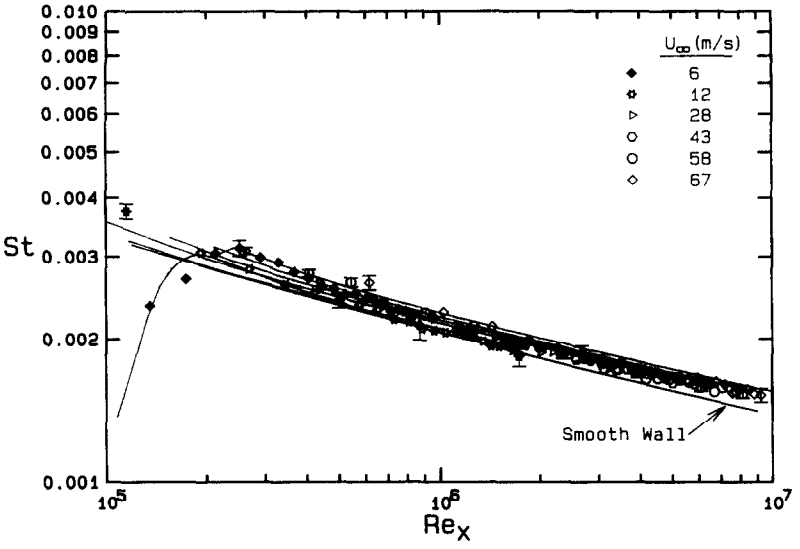

FIG. 11. The THTTF Stanton number data and predictions vs Re_x for the $L/d_0 = 10$ rough surface.

ent is represented by the acceleration parameters K_t for the equilibrium cases and K for the non-equilibrium case, where $K_t = (r/U_\infty)\,dU_\infty/dx$ and $K = (\nu/U_\infty^2)\,dU_\infty/dx$. For the two equilibrium cases $K_t = 0.15 \times 10^{-3}$ and 0.29×10^{-3} and the non-equilibrium case $K = 0.28 \times 10^{-3}$ shown in Fig. 12, the discrete element predictions are in excellent agreement with the data.

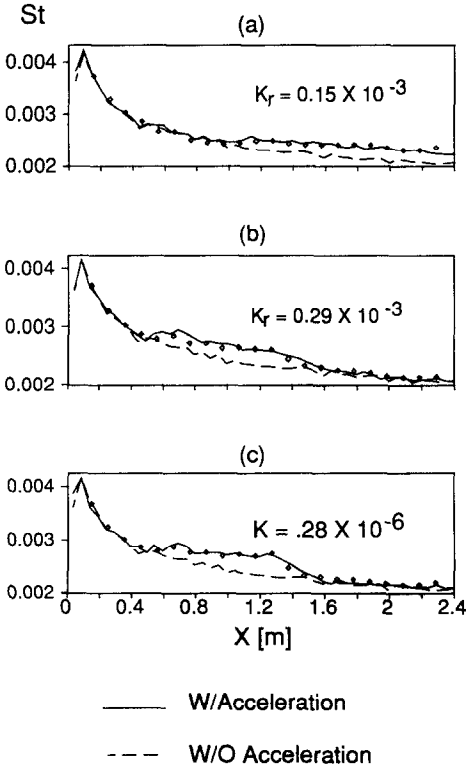

FIG. 12. Equilibrium and non-equilibrium accelerated Stanton number data reported in ref. [17] and predictions for the Stanford surface.

Comparisons of the predictions from the discrete element method and data from the four different rough surfaces for zero pressure gradient and favorable pressure gradient cases and over the range of smooth, transitionally rough and fully rough regimes show that the predictions are in excellent agreement with data for all cases. It is especially encouraging that the discrete element model properly predicts the somewhat different behavior of the data from the Stanford and THTTF surfaces in St vs Δ_2/r and St vs Re_x coordinates.

Characterization of roughness flow regimes

As discussed previously, various measures for classification of flow regimes based on observations of fluid dynamics and heat transfer behaviors of rough-wall data have been presented in the literature. The only non-sandgrain computational delimiter for identification of rough-wall flow regimes available is that given in ref. [29], where it was proposed that the ratio of the apparent shear stress due to the roughness elements to the total apparent shear stress ($R_\tau = \tau_R/\tau_T$) be used to distinguish between aerodynamically smooth, transitionally rough and fully rough regimes. Scaggs *et al.* [8], based on their extensive fluid dynamics data set and the corresponding calculations of τ_T and τ_R made using the discrete element model, suggested that a value of R_τ about 0.6 might be considered as an appropriate boundary between the transitionally rough and fully rough flow regimes. This measure is based only on the fluid dynamics character of rough-wall flows.

An analogous parameter based on the effects of roughness elements on the heat transfer characteristics of rough-wall flows is the ratio of the rate of

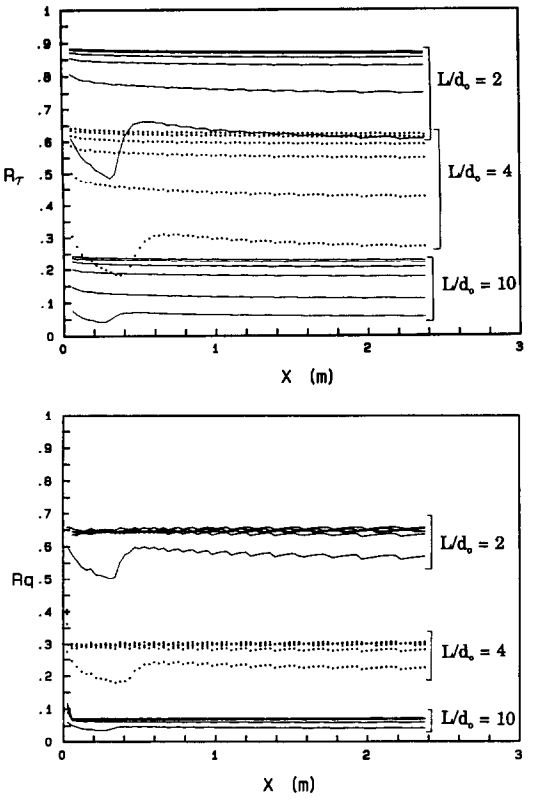

FIG. 13. Values of R_τ and R_q calculated using the discrete element method for $U_\infty = 6$, 12, 28, 43, 58 and 67 m s^{-1} for the THTTF rough surfaces.

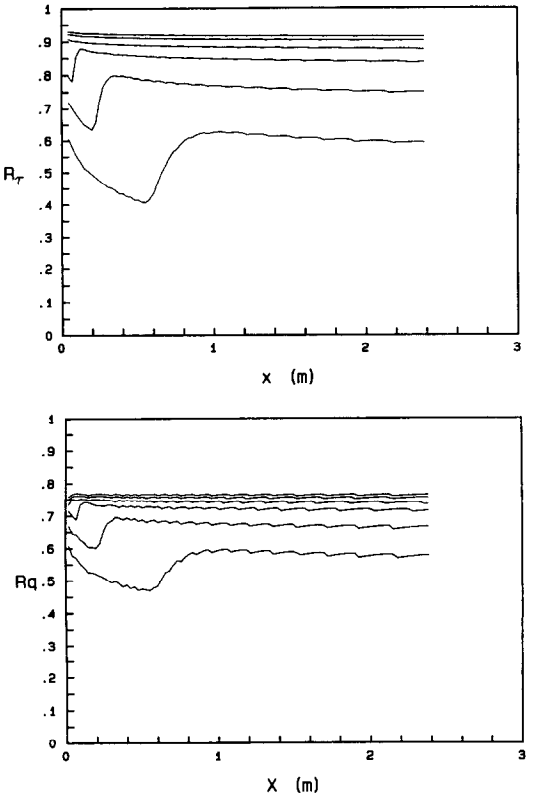

FIG. 14. Values of R_τ and R_q calculated using the discrete element method for $U_\infty = 9$, 16, 27, 40, 58 and 74 m s^{-1} for the Stanford rough surface.

heat transfer from the roughness elements to the fluid to the total rate of heat transfer from the surface to the fluid, $R_q = q_R/q_T$. Figure 13 shows a plot of calculated values of R_q using the refined roughness element energy transport model in the discrete element method for the three THTTF rough surfaces. Also presented for comparison are calculated values of R_τ. A similar plot is presented in Fig. 14 for the zero pressure gradient Stanford data sets.

The behavior of R_q seems to mirror the behavior of the Stanton number data in Re_x coordinates. For each THTTF surface, the R_q values collapse to essentially a constant value except for the lowest freestream velocities of 6 and 12 m s^{-1}. For the zero pressure gradient data sets from the Stanford surface, the collapse of R_q to a constant value appears to occur at a slightly higher freestream velocity than for the THTTF surfaces.

SUMMARY AND CONCLUSIONS

As a result of this experimental investigation, Stanton number data are now available over a wide range of Reynolds numbers for the three well-defined THTTF rough surfaces in addition to the previously reported data for the somewhat similar Stanford rough surface. This vastly expanded data set allows observations and conclusions about rough-wall heat transfer behavior to be made which were not apparent in the data from the single Stanford surface.

It appears that for a given surface, Stanton number data in Re_x coordinates approach an asymptotic curve as freestream velocity is increased, becoming a function of Re_x alone (as is the case for smooth wall turbulent flows). The results from the three THTTF rough surfaces indicate that there is a different asymptotic St–Re_x curve for each surface, with Stanton number at a given Re_x increasing with decreasing roughness spacing, that is, as the surface becomes 'rougher'.

The asymptotic curve for the Stanford surface falls between those of the $L/d_0 = 2$ and 4 THTTF surfaces. This seems to indicate that the magnitude of the roughness effect on heat transfer increases with decreased roughness element spacing only up to some 'roughest' spacing. As roughness element spacing is decreased more (and approaches the most densely packed configuration), the magnitude of the roughness effect on heat transfer diminishes. This is in agreement with the trends shown by Schlichting's [2] data for roughness effects on skin friction as a function of roughness element spacing.

The Stanton number approach to the asymptotic curve as freestream velocity increases does not seem to correlate with a change from the transitionally rough

Table 1. Summary of flow regime classifications based on u'^2 behavior and calculated R_τ values, and observed heat transfer behavior for the three rough THTTF surfaces

	$L/d_0 = 10$			$L/d_0 = 4$			$L/d_0 = 2$		
U_∞ (m s^{-1})	u'^2	R_τ	St vs Re_x	u'^2	R_τ	St vs Re_x	u'^2	R_τ	St vs Re_x
6	TR	S/Lower TR	NA	TR	TR	NA	TR	Lower FR	NA
12	TR	TR	NA	TR	TR	NA	Upper TR/ Lower FR	FR	NA
28	TR	TR	A	FR	Upper TR/ Lower FR	A	FR	FR	A
43	—	TR	A	FR	Lower FR	A	FR	FR	A
58	—	TR	A	FR	Lower FR	A	FR	FR	A
67	—	TR	A	—	Lower FR	A	—	FR	A

S, smooth; TR, transitionally rough; FR, fully rough; —, no data taken; A, asymptotic; NA, non-asymptotic.

flow regime to the fully rough flow regime as defined based on the fluid dynamics behavior of the turbulent boundary layers. This is shown in Table 1, which presents for the three THTTF rough surfaces a summary of flow regime classifications based on the behavior of u'^2 profiles and the calculated R_τ values [37] along with the observed heat transfer behavior (asymptotic or non-asymptotic) in St vs Re_x coordinates.

The data from the three rough THTTF surfaces, taken together with the data from the Stanford surface, show quite clearly that data for a given surface viewed in Stanton number vs enthalpy thickness coordinates do not collapse to a single curve in the regime determined as fully rough based on fluid dynamics characteristics. Such behavior had been postulated based only on observations of the data from the Stanford surface, but this postulate cannot be sustained.

The results of comparisons of the heat transfer data with predictions using the discrete element method with the refined roughness element energy transport model (equation (13)) are very encouraging. Excellent agreement is observed for the four rough surfaces over the range of flow regimes from aerodynamically smooth to transitionally rough to fully rough and for both zero pressure gradient and favorable pressure gradient cases. The Stanton number predictions show the proper trends in both Re_x and enthalpy thickness coordinates and also the differences in behavior between the Stanford surface and the THTTF surfaces in these coordinates.

Acknowledgements—This work was supported by the U.S. Air Force Office of Scientific Research (Research Grant AFOSR-86-0178); the experimental apparatus was acquired under grant AFOSR-85-0075. The authors gratefully acknowledge the interest and encouragement of Capt. Hank Helin of AFOSR.

REFERENCES

1. J. Nikuradse, Stromungsgesetze in rauhen rohren, *VDI ForschHft.* 361 (1933). (Also: Laws of flow in rough pipes, NACA TM 1292.)
2. H. Schlichting, Experimentelle untersuchungen zum rauhigkeits-problem, *Ing.-Arch.* **VII**(1), 1–34 (1936). (Also: Experimental investigation of the problem of surface roughness, NACA TM 832.)
3. A. E. Perry and P. N. Joubert, Rough-wall boundary layers in adverse pressure gradients, *J. Fluid Mech.* **17**, 193–211 (1963).
4. D. E. Nestler, Compressible turbulent boundary layer heat transfer to rough surfaces, ASME Paper 70-742 (1970).
5. T. Cebeci and K. C. Chang, Calculation of incompressible rough-wall boundary-layer flows, *AIAA J.* **16**, 730–735 (1978).
6. H. W. Coleman, B. K. Hodge and R. P. Taylor, Generalized roughness effects on turbulent boundary layer heat transfer, AFATL-TR-83-90 (1983).
7. H. W. Coleman, B. K. Hodge and R. P. Taylor, A reevaluation of Schlichting's surface roughness experiment, *J. Fluids Engng* **106**, 60–65 (1984).
8. W. F. Scaggs, R. P. Taylor and H. W. Coleman, Measurement and prediction of rough wall effects on friction factors in turbulent pipe flow, Report TFD-88-1, Mech. and Nucl. Engng Dept., Miss. State Univ. (1988).
9. W. F. Scaggs, R. P. Taylor and H. W. Coleman, Measurement and prediction of rough wall effects on friction factor—uniform roughness results, *J. Fluids Engng* **110**, 385–391 (1988).
10. W. Nunner, Heat transfer and pressure drop in rough tubes, *VDI ForschHft.* 455, Series B, **22**, 5–39 (1956), English Translation, A.E.R.E. Library/Transactions 786 (1958).
11. D. F. Dipprey and R. H. Sabersky, Heat and momentum transfer in smooth and rough tubes at various Prandtl numbers, *Int. J. Heat Mass Transfer* **6**, 329–353 (1963).
12. N. S. Sood and V. K. Johnson, Some correlations for resistances to heat and momentum transfer in the viscous sublayer at rough walls, *Trans. ASME, J. Heat Transfer* 488–494 (1969).
13. R. H. Norris, Some simple approximate heat transfer correlations for turbulent flow in ducts with surface roughness. In *Augmentation of Convective Heat and Mass Transfer*. ASME, New York (1971).
14. A. M. Yaglom and B. A. Kader, Heat and mass transfer between a rough wall and turbulent fluid flow at high Reynolds and Peclet number, *J. Fluid Mech.* **62**, 601–623 (1974).
15. J. M. Healzer, The turbulent boundary layer on a rough, porous plate: experimental heat transfer with uniform blowing, Ph.D. Dissertation, Mech. Engng Dept., Stanford Univ. (1974). (Also Report HMT-18.)
16. M. M. Pimenta, The turbulent boundary layer: an exper-

imental study of the transport of momentum and heat with the effect of roughness, Ph.D. Dissertation, Mech. Engng Dept., Stanford Univ. (1975). (Also Report HMT-21.)
17. H. W. Coleman, Momentum and energy transport in the accelerated fully rough turbulent boundary layer, Ph.D. Dissertation, Mech. Engng Dept., Stanford Univ. (1976). (Also Report HMT-24.)
18. P. M. Ligrani, The thermal and hydrodynamic behavior of thick rough-wall turbulent boundary layers, Ph.D. Dissertation, Mech. Engng Dept., Stanford Univ. (1979). (Also Report HMT-29.)
19. H. W. Liepmann and F. E. Goddard, Note on the mach number effect upon the skin friction of rough surfaces, *J. Aeronaut. Sci.* **24,** 784 (1957).
20. M. J. Lewis, An elementary analysis for predicting the momentum and heat transfer characteristics of a hydraulically rough surface, *J. Heat Transfer* **97,** 249–254 (1975).
21. M. L. Finson, A Reynolds stress model for boundary layer transition with applications to rough surfaces, AFOSR-TR-76-0322 (1975).
22. J. C. Adams and B. K. Hodge, The calculation of compressible transitional turbulent and relaminarizational boundary layers over smooth and rough surfaces using an extended mixing-length hypothesis, AIAA Paper 77-682 (1977).
23. M. L. Finson and P. K. S. Wu, Analysis of rough wall turbulent heating with applications to blunted flight vehicles, AIAA Paper 79-008 (1979).
24. M. L. Finson and A. S. Clark, The effects of surface roughness character on turbulent reentry heating, AIAA Paper 80-1459 (1980).
25. T. C. Lin and R. J. Bywater, The evaluation of selected turbulence models for high-speed rough wall boundary layer calculations, AIAA Paper 80-0132 (1980).
26. M. L. Finson, A model for rough wall turbulent heating and skin friction, AIAA Paper 82-0199 (1982).
27. G. H. Christoph, Law of the wall analysis for turbulent heating on rough surfaces, AIAA Paper 82-0197 (1982).
28. G. H. Christoph and R. N. Pletcher, Prediction of rough-wall skin friction and heat transfer, *AIAA J.* **21**(4), 509–515 (1983).
29. R. P. Taylor, H. W. Coleman and B. K. Hodge, A discrete element prediction approach for turbulent flow over rough surfaces, Report TFD-84-1, Mech. and Nucl. Engng Dept., Miss. State Univ. (1984).
30. R. P. Taylor, H. W. Coleman and B. K. Hodge, Prediction of turbulent rough-wall skin friction using a discrete element approach, *J. Fluids Engng* **107,** 251–257 (1985).
31. J. C. Adams, Numerical calculations of the subsonic and transonic turbulent boundary layer on an infinite yawed airfoil, AEDC-TR-73-112 (1973).
32. H. W. Coleman, M. H. Hosni, R. P. Taylor and G. B. Brown, Smooth wall qualification of a turbulent heat transfer test facility, Report TFD-88-2, Mech. and Nucl. Engng Dept., Miss. State Univ. (1988).
33. W. C. Reynolds, W. M. Kays and S. J. Kline, Heat transfer in the turbulent incompressible boundary layer, parts I, II, and III, NASA MEMO 12-1-58W, 12-2-58W, and 12-3-58W (1958).
34. R. G. Eckert and R. J. Goldstein, *Measurements in Heat Transfer*, 2nd Edn. McGraw-Hill, New York (1976).
35. Measurement Uncertainty, ANSI/ASME PTC 19.1-1985, Part I (1986).
36. H. W. Coleman and W. G. Steele, *Experimentation and Uncertainty Analysis for Engineers*. Wiley, New York (1989).
37. M. H. Hosni, H. W. Coleman and R. P. Taylor, Measurement and calculation of surface roughness effects on turbulent flow and heat transfer, Report TFD-89-1, Mech. and Nucl. Engng Dept., Miss. State Univ. (1989).
38. W. M. Kays and M. E. Crawford, *Convective Heat and Mass Transfer*, 2nd Edn. McGraw-Hill, New York (1980).
39. R. P. Taylor, H. W. Coleman, M. H. Hosni and P. H. Love, Thermal boundary condition effects on heat transfer in the turbulent incompressible flat plate boundary layer, *Int. J. Heat Mass Transfer* **32,** 1165–1174 (1989).

MESURE ET CALCUL DU TRANSFERT THERMIQUE SUR PAROI RUGUEUSE EN COUCHE LIMITE TURBULENTE

Résumé—Des résultats expérimentaux de nombre de Stanton pour des écoulements turbulents à couche limite sur des surfaces aérodynamiquement lisses, moyennement rugueuses et pleinement rugueuses sont présentés pour quatre surfaces dont trois rugueuses et une lisse. Les surfaces rugueuses sont composées d'hémisphères de 1,27 mm de diamètre espacées selon un arrangement en quinconce avec un pas de 2, 4 et 10 diamètres. Les données de nombre de Stanton sont reportées pour un gradient de pression nul dans un écoulement d'air qui donne Re_x allant jusqu'à 10^7. Ces données sont comparées à des résultats antérieurement publiés pour une surface rugueuse similaire et on montre que quelques conclusions sur le transfert thermique avec cette seule surface rugueuse ne s'étendent pas aux nouvelles surfaces. Un modèle amélioré et une méthode numérique sont aussi présentés. Des calculs sont comparés aux données expérimentales dans le cas d'écoulements à pression constante ou accélérés, et on montre que les prédictions s'accordent bien aux données.

MESSUNG UND BERECHNUNG DES WÄRMEÜBERGANGS IN DER TURBULE. GRENZSCHICHT EINER RAUHEN WAND

Zusammenfassung—Es werden experimentell bestimmte Stanton-Zahlen für aerodynamisch glatte und vollständig rauhe, turbulente Grenzschichtströmungen sowie für solche im Übergangsgebiet vorgestellt, und zwar für vier Oberflächen: drei rauhe und eine glatte. Die rauhen Oberflächen sind aus Halbkugeln mit dem Durchmesser 1,27 mm aufgebaut, die in versetzter Anordnung im gegenseitigen Abstand von 2, 4 und 10 Durchmessern auf einer ansonsten glatten Oberfläche befestigt sind. Es werden Ergebnisse in Gestalt der Stanton-Zahl für eine inkompressible turbulente Grenzschichtströmung aus Luft beim Druckabfall 0 für Re_x bis zu 10 000 000 angegeben. Diese Daten werden mit kürzlich veröffentlichten Ergebnissen von einer weiteren, ähnlich rauhen Oberfläche verglichen. Dabei zeigt sich, daß einige Schlußfolgerungen bezüglich des Wärmeübergangs, die auf den Ergebnissen jener einzelnen rauhen Oberfläche basieren, sich nicht auf diese neuen Oberflächengeometrien ausdehnen lassen. Ein verbessertes Modell für den Energietransport an Rauhigkeitselementen wird vorgeschlagen, das in das kürzlich veröffentlichte Verfahren einzusetzen ist. Die Ergebnisse der Berechnung werden mit Daten von den vier rauhen Oberflächen mit definierten Rauhigkeitselementen verglichen, und zwar sowohl für konstanten Druck als auch für beschleunigte Strömung. Dabei zeigt sich hervorragende Übereinstimmung.

ИЗМЕРЕНИЯ И РАСЧЕТЫ ТЕПЛОПЕРЕНОСА ОТ ШЕРОХОВАТЫХ СТЕНОК В ТУРБУЛЕНТНОМ ПОГРАНИЧНОМ СЛОЕ

Аннотация—Получены экспериментальные результаты по числу Стэнтона для аэродинамически гладкого, неустановившегося и полностью турбулентного течений в пограничном слое вблизи четырех поверхностей—трех шероховатых и одной гладкой. Шероховатые поверхности образованы полусферами диаметром 1,27 мм, расположенными в шахматном порядке на расстояниях, равных, соответственно, 2, 4 и 10 диаметрам оснований, причем остальные поверхности были гладкими. Представлены данные по числу Стэнтона для турбулентных течений несжимаемого воздуха в пограничном слое с нулевым градиентом давления для значений Re_x вплоть до 10 000 000. Эти данные сопоставлены с ранее опубликованными результатами для другой поверхности с аналогичной шероховатостью, и показано, что некоторые выводы о характере теплопереноса, основанные на полученных данных для этой единичной шероховатой поверхности, не распространяются на описываемые новые геометрии поверхностей. Предложена также усовершенствованная модель переноса энергии от элемента шероховатости, которая может использоваться в ранее предложенном методе определения дискретных элементов. Проведено сравнение расчетов с результатами, полученными для четырех шероховатых поверхностей с хорошо выраженными элементами шероховатости как в случае течения с постоянным давлением, так и в случае ускоряющегося течения, и показано, что расчеты очень хорошо согласуются с экспериментальными данными.